Diyala Journal of Engineering Sciences

Journal homepage: https://djes.info/index.php/djes

ISSN: 1999-8716 (Print); 2616-6909 (Online)

# Experimental and Numerical Investigations on the Heat Transfer of a Helical Coil Heat Exchanger Utilized $\alpha - Al_2O_3$ Nanofluid

Mustafa S. Abdullah[1,2*], Adnan M. Hussein[1]

[1]Department of Power Mechanics Techniques, Northern Technical University, 36001 Kirkuk, Iraq
[2]Automotive Technology Engineering Department, Erbil Polytechnic University, 44001 Erbil, Iraq

**ARTICLE INFO**

***Article history:***
Received March 1, 2023
Revised July 3,2023
Accepted July 14,2023,
Available online September 3, 2023

***Keywords:***
Nanofluid
Shell and coil heat exchanger
Thermal performance
Pitch ratio
Nusselt number

**ABSTRACT**

This study focused on investigating the impact of α-$Al_2O_3$ nanoparticles of volume concentration 0.1% on heat transfer in shell and helical coiled tube heat exchangers. The objective was to analyze the influence of geometrical characteristics, specifically the coil pitch, on the Nusselt numbers of both sides using a combination of numerical simulations and experimental methods. The working fluid for the hot side was water. The research encompassed an examination of the friction factor for three different coils, exploring the effects of pitch spacing on heat transfer, and assessing the influence of nanoparticles on heat transfer on the inner side of the coil. The findings of the current work indicated significant improvements in heat transfer parameters when employing water-α-$Al_2O_3$ nanoparticles as the cold fluid. Comparing this heat exchanger to one without the inclusion of α-$Al_2O_3$ nanoparticles revealed a remarkable efficiency enhancement of 7.68 percent. This increase strongly suggests a notable acceleration in the rate of heat transmission within the heat exchanger. Overall, this study provides valuable insights into the utilization of α-$Al_2O_3$ nanoparticles in enhancing heat transfer in shell and helical coiled tube heat exchangers. The results highlight the potential benefits of incorporating nanoparticles into such systems, leading to improved performance and more efficient heat exchange processes.

## 1. Introduction

To move heat from one medium to another, heat exchangers are used. These add-ons may improve productivity and safeguard machinery. Refrigeration, the food industry, heat recovery systems, HVAC, power plants, and nuclear reactors are just some of the numerous places shell and tube heat exchangers are used [1-4]. The helically coiled tube is preferable to the straight tube because of its decreased heat transfer coefficient, improved heat capacity, and less pressure loss. These heat exchangers have a better heat transfer coefficient than straight tubes because centrifugal force creates a secondary flow that moves in the same direction as the primary flow [5].

The use of nanofluids in a secondary cooling loop was the subject of a pilot study [6]. Where $Al_2O_3$ was utilized, mass flow rates of 40-80 g/s were employed, and input temperatures of 30-40 °C were used. The efficiency of the new system was improved by including a $Al_2O_3$ nanofluid in the secondary loop. In cases when a higher COP was possible, it peaked at 6.5. It was found that the nanofluid had a considerably higher heat conductivity than regular water. Nanofluid ($Al_2O_3$) was used in an exergy investigation [7] using helical and conical tube heat exchangers with 0.3, 0.6, and 1.0

* Corresponding author.
E-mail address: Mustafa.Sabah@ntu.edu.iq
DOI: 10.24237/djes.2023.16306

volumetric concentrations. Increases in particle size concentration lead to a rise in the nanofluid's overall heat transfer coefficient, convective heat transfer coefficient, coil-side Nusselt number, reactivity, and exothermic efficiency compared to pure water. Increasing the coil's twist from 0.052 to 0.0202 improved $U_{ov}$, $h_t$, $Nu_t$, ε, and $\eta_{ex}$. [8] examined heat transfer in concentric annular pipes of different forms (Circular, Square, Diamond, Triangular, Rectangular, and Elliptic) using pure water. Elliptic and circular pipes transferred heat 40% and 37% quicker than other designs. Al2O3-H2O and H2O-SiO3 nanofluids demonstrated a 6% greater heat transfer coefficient than pure water at low pressure. Finally, the study examined how inclination angle (θ) and aspect ratio (AR) affect heat transport and annular gap pressure, finding an ideal design at AR = 8 and $\theta = 90^o$. [9] looked at LMTD time series and heat transfer efficiency using helical shell heat exchangers and Al2O3 nanoparticles at a volumetric concentration of 0.1%. When $Al_2O_3$ nanoparticles (at a concentration of 0.1%) were added, and the LMTD time series was shown to decrease. As a cold solution for a heat exchanger, water and alumina are 2.2% more effective than distilled water.[10] studied shell and spiral tube heat exchange utilizing $Al_2O_3$ nanofluid concentrations of 0.1%, 0.4%, and 0.8% by volume. The findings indicate that the overall coefficient of heat transfer, pressure drop, internal coefficient of heat transfer, and internal Nusselt number is 30%, 15%, and 56% more than that of water with a concentration of 0.8% by volume. As the viscosity of a fluid increases, its particle size gets more concentrated, resulting in a pressure reduction. The impact of surfactants at volumetric concentrations of 0.1-0.4% on the heat transfer of alumina-silver nanoparticles in a spiral heat exchanger was studied [11]. Adding 0.2% alumina hybrid silver particles and 0.1% sodium dodecyl sulfate anionic surfactants boosted thermal efficiency by 16% compared to pure water. Nanofluids ($Al_2O_3$ and $TiO_2$) with a volumetric concentration of 0.25–1.0% and 500–4500 Reynolds numbers were used in experimental research using helical tubes [12]. As a result of $Al_2O_3$ nanofluids' superior thermal conductivity and smaller size in comparison to $TiO_2$ nanoparticles, heat transmission is improved. Both experimentally and statistically, [13] investigated the influence of a water-based $Al_2O_3$ nanofluid on heat transport in a spirally coiled tube at varying Reynolds numbers. At Reynolds numbers 200, 600, and 1500, heat transfer in $Al_2O_3$ nanofluids are enhanced. At low Reynolds numbers, the $Al_2O_3$ nanofluids cooled the tube wall more than water using polygonal geometries with varying coil rotations, [14] conducted a computational investigation of the heat transfer performance of a helical heat exchanger operating with water-based nanofluids ($Al_2O_3$, $CuO_2$, $SiO_2$, ZnO), at a volumetric concentration (4%). The findings indicate that utilizing a double-sided head design and rotating 30 coils may increase heat transfer by as much as 80%. Al2O3 has a greater heat transfer rate, much as SiO2.  A numerical study of turbulent heat transfer and the flow of nanofluids in a spiral heat exchanger is presented [15]. Water-based nanofluids with 1.5, 3, 4, and 5% volume concentrations of $Al_2O_3$, CuO, and $SiO_2$. At a high Reynolds number, the researcher found that a five-lobed cross-section increased the Nusselt number and decreased the pressure by 4.8% and 3.7%, respectively. Thermally, three-lobed designs are the most effective. When compared to other materials, CuO nanofluid had the highest thermal efficiency. In addition, the thermal performance of $Al_2O_3$, CuO, and $SiO_2$ nanofluids in a spiral heat exchanger has been analyzed [16] [17]. numerically evaluated $Al_2O_3$/water, CuO/water, and SiO2/water nanofluids (2%, 4%, and 6% volume fractions) in different channel geometries under uniform and varying hot surface temperatures. Elliptical cross-sectioned channels had double the heat transmission coefficient of airfoil pipe, square, circle, and ellipse at the same hot surface temperature. $Al_2O_3$ dispersion enhanced heat transfer by 15%. Higher nanofluid fractions improved heat transmission with low-pressure decreases. [18] investigated temperature variation in a shell and single/double coil heat exchanger using experimental and numerical analysis. They examined different coil pitches and hot/cold water flow rates on the coil's outer surface. The results show a decrease of 3.07% in hot outlet temperature for double coils at a 2.5L/min hot water flow rate. Increasing coil pitch improved hot fluid-coil contact and reduced hot fluid outlet temperature. Centrifugal forces in double-coil heat exchangers with different coil pitches significantly affected secondary flow. For the same conditions [19] found that the Nusselt number in a double coil was 18.2% higher than a single coil at 1800 Reynolds number on the shell side. The exit temperature difference increased by less than 1% and 8%, respectively, when the coil diameter was raised by 11%, from 0.016 to 0.022. CuO has the highest Reynolds number of any aqueous nanofluid. Furthermore, between 2% and 4% concentration, the nanofluid modulus is at its lowest. Lobed helical coils in $Al_2O_3$ nanofluids were investigated in laminar flow [20]. The results show that the n=6 coil has the highest Nusselt number and the least friction. Increases in coil diameter led to increases in both the Nusselt number and friction factor and the Nusselt number of the $Al_2O_3$ nanofluid was greater than that of the base fluid and grew with increasing nanoparticles volume using Reynolds numbers between 10,000 and 60,000 and coil curvatures between 0.032 and 0.052 [21], they analyzed the turbulent flow of $Al_2O_3$ nanofluids in helically coiled, hybrid rectangular tubes subjected to continuous wall convective flow at volumetric concentrations (1-4%). The nanoparticle density and curvature outcomes were better heat transmission and reduced friction pressure. A numerical investigation of $Al_2O_3$ nanofluid in helical heat exchangers have been conducted [22]. Adding nanoparticles at concentrations of 0.2% and 0.3% increases heat transmission by 14% and 18%. Raising the particle concentration improves heat transmission on both the coil and shell sides and throughout the system. [23] conducted a numerical investigation utilizing (HCHEs). The first test used water, whereas the second substituted $Al_2O_3$ for both the coiled and outer layers. Due to the high specific heat of $Al_2O_3$, the findings demonstrated that the coefficient of heat transfer is greatly enhanced when fluid flows within a helically coiled tube as opposed to a straight one. [24] looked into the effects of different Nanofluid volume concentrations on the convective heat transfer and pressure drop of water/$Al_2O_3$ Nanofluid flowing in helical heat exchangers (0.5 wt %, 1.0 wt %, and 2.0 wt %). The diameters of the coils range from 0.18 to 0.24 to 0.30 meters. Increases in the curvature ratio result in a greater friction factor under continuous pressure decrease. Helically corrugated tubes filled with Al2O3 nanofluids were subjected to a computational study of turbulent heat transport [25]. At 10,000-40,000 Reynolds numbers and volumetric concentrations of 0.3-0.7%. Heat transmission was shown to be enhanced with increasing nanofluid size. Heat transfer is enhanced by 21% and 58%, respectively, when nanofluid is used at a volume concentration of 2% and 4%. [26] studied numerically the evaluated flow structure and coil friction factor and wall shear stress using STD(k-w) and STD(k-ϵ)). Three identical 0.005m and 0.04m coils were tested. The initial pitch variations for the first, second, and third models were 0.01 m, 0.05 m, and 0.25 m. In turbulent flows, the Dean number reduced the coil friction factor more than the pitch size.

Few studies have examined how changing the coil pitch in a helically coiled heat exchanger affects the thermal efficiency of operating with $\alpha - Al_2O_3$ nanofluids in distilled water. Therefore, a 3D helically coiled heat exchanger working with a $\alpha - Al_2O_3$ nanofluid based on distilled water has been the subject of theoretical and experimental investigation in this study. Coil intake temperature, shell/coil flow rate, coil diameter, and Coil pitch ratio have all been considered to provide optimal heat transmission in the heat exchanger. The findings show that the efficiency of the heat exchanger is drastically increased by using a nanofluid based on $\alpha - Al_2O_3$.

## 2. Experimental methodology

### *2.1 Test rig*

The experimental setup is depicted schematically in Fig. 1 and consists of a tank, pumps, heat exchangers, a flow meter, a pressure gauge, and a temperature controller. Coil 1, Coil 2, and Coil 3 are made of copper tubes with internal and external diameters of 8.5 mm and 9 mm, respectively, and lengths of 6.224 m, 3.417 m, and 2.39 m, respectively. Copper tubes are bent on a cylindrical track of specified diameter to produce coil pitches of 20 mm, 35 mm, and 50 mm, respectively, using salt inside the copper tube to prevent bending or cracking. Then rinse with hot water to remove the salt. The shell is made of U-PVC tubing measuring 152.4 millimeters in diameter. The heat exchanger is finally separated using fiberglass that is 3 cm thick. A temperature controller keeps the temperature within the specified range when the heater heats the water. The heated fluid then passes through the heat exchanger at T1 and leaves at T2 respectively. A centrifugal pump, type QB50-0.15HP Pipe Pump, pumps the cold nanofluid. The cold nanofluid then passes through the flowmeter, entering the coil side of the heat exchanger at T3 temperature and leaving at T4 temperature. All temperatures are obtained through the Data Logger using thermocouples of the K type, with an uncertainty of ±2.5°C. The heat exchanger's outside is wholly insulated to lower heat loss.

*2.2 Nanofluid preparation*

Nanoparticles of 99.9+% pure 50 nm α-$Al_2O_3$ were employed in a helical coil tube study of heat exchange. In Fig. 2, we see scanning electron microscopy (SEM) pictures of an α-$Al_2O_3$ nanoparticle, which provide details about its form. This study utilized optimal mixing and sonication to maintain nanoparticle dispersion throughout the base fluid. The volume content of the α-$Al_2O_3$/water nanofluid is 0.1 vol%. In order to control the concentration of the α-$Al_2O_3$ nanofluid in a given volume, the weight of the fluid is determined using an analytical balance. The nanofluids are made homogenous and stable by 1 hour of ultrasonic homogenization using a VEVOR ultrasonic and 30 minutes of stirring with a SNIJDERS magnetic stirrer.

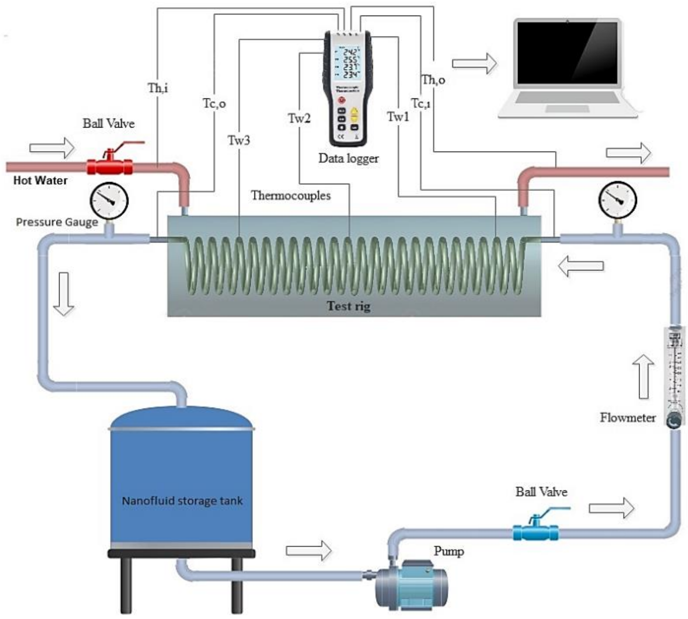


**Figure 1.** Illustration diagram of the test rig

Sedimentation of nanoparticles was detected after ultrasonication in this study. The stability time of the nanoparticles and the time needed for their dispersal throughout the water were calculated by continuously monitoring the nanofluid until the particle separation phase began. In experiments, it was found that a nanofluid's consistency could be sustained for around 72 hours at a volume content of 0.1%. Fig. 3 visually represents the procedure employed to monitor the nanofluid sample.

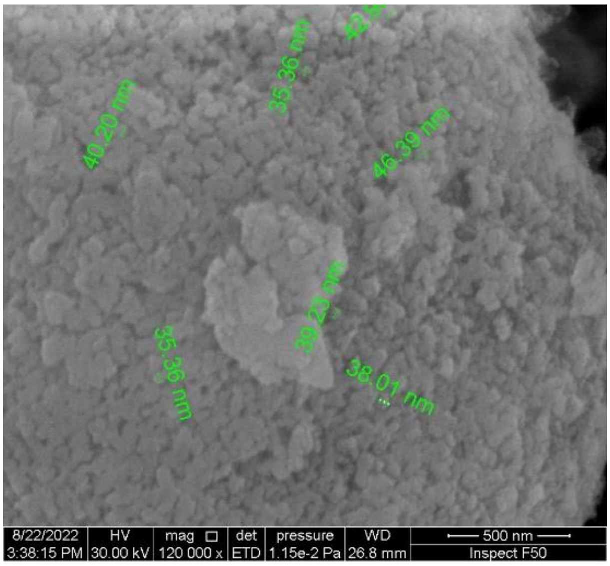


**Figure 2.** SEM images of $\alpha - Al_2O_3$.

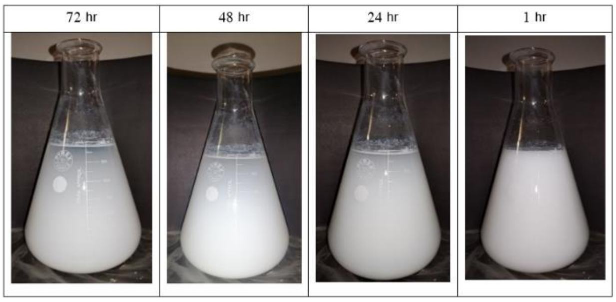


**Figure 3.** Time-lapse photograph of α- $Al_2O_3$ sample stability.

**Table 1**: contains a list of water and $\alpha - Al_2O_3$'s Thermo-physical characteristics [25].

| Fluid | Density $(kg/m^3)$ | specific heat $(J/kg.K)$ | Thermal conductivity $(W/m.K)$ |
|---|---|---|---|
| Water | 997 | 4179 | 0.6 |
| $\alpha$-$Al_2O_3$ | 3700 | 880 | 46 |

### *2.3 Uncertainty calculation*

Uncertainty estimation plays an essential role in any experimental activity. The resulting data may be seen in Table 2. The most significant error percentages for the Nu and Reynolds values are 3.92% and 3.72%, respectively.

### *2.4 Data analysis*

Sensor data is utilized to calculate the Nusselt number, heat transfer coefficient, and heat transfer rate for the whole experiment. As a result, the average heat transfer rate may be calculated as follows [27]:

$$q_h = \dot{m}_h \times Cp_{eff,h} \times (Th_i - Th_o) \quad (1)$$

$$q_c = \dot{m}_c \times Cp_{eff,c} \times (Tc_o - Tc_i) \quad (2)$$

**Table 2:** The value of experimental uncertainty

| **Parameters** | **Formulas** [28] | **Results** |
|---|---|---|
| $U_{Re}$ | $\sqrt{\left(\frac{\delta \dot{m}_c}{\dot{m}_c}\right)^2 + \left(\frac{-\delta d_i}{d_i}\right)^2 + \left(\frac{-\delta \mu_{eff,c}}{\mu_{eff,c}}\right)^2}$ | 3.92% |
| $U_{Nu_c}$ | $\sqrt{\left(\frac{\delta q_{avg}}{q_{avg}}\right)^2 + \left(\frac{\delta D_h}{D_h}\right)^2 + \left(\frac{-\delta A_s}{A_s}\right)^2 + \left(\frac{-\delta T_w}{T_{w,avg} - T_{c,ang}}\right)^2 + \left(\frac{-\delta T_{c,avg}}{T_{w,ave} - T_{c,avg}}\right)^2}$ | 3.72% |

$$q_{avg} = \frac{q_h + q_c}{2} \quad (3)$$

Where $q_h$ refers to the heat transfer from the shell, and $q_c$ refers to the heat transfer from the coil. In addition, the average rate of heat transfer is denoted by $q_{avg}$, while the rate of mass flow is denoted by $\dot{m}$.

To get the overall heat transfer coefficient, we use Eq. (4), with F=1 for counter-flow [29]:

$$U_i = \frac{q_{avg}}{A_s \times LMTD \times F} \quad (4)$$

And

$$LMTD = \frac{(Th_i - Tc_o) - (Th_o - Tc_i)}{\ln\left(\frac{(Th_i - Tc_o)}{(Th_o - Tc_i)}\right)} \quad (5)$$

LMTD is the logarithmic mean temperature difference, and (As) is the inner tube's heat transfer area. The coil side Nusselt number is calculated using this formula:

$$Nu_c = \frac{h_i \times d_i}{k_{eff,i}} \quad (6)$$

And [30]:

$$D_h = 4\frac{\left[\left(\frac{\pi}{4}\ (D_{sh,i})^2 \times L_{sh}\right) - \left(\frac{\pi}{4}\ (d_{c,o})^2 \times L_c\right)\right]}{\left[(\pi D_{sh,i} L_{sh}) + (\pi d_{c,o} L_c)\right]} \quad (7)$$

The hydraulic diameter is denoted by $D_h$. Additionally, the heat transfer coefficient of the coil and its thermal conductivity is denoted by $h_i$ and $k_i$, respectively.

T he pressure difference (ΔP) is calculated using a pressure gauge [31].

$$\Delta P = P_{in} - P_{out} \quad (8)$$

Calculate the friction factor for the coil tube from the following equation [32]:

$$f = \frac{\Delta P}{\left(\frac{L}{d_i}\right)\left(\frac{\rho_{eff} u_i^2}{2}\right)} \quad (9)$$

Where $L$, $d_i$, $\rho_{eff}$ and $u_i$ are the coil length, inner coil diameter, density, and flow velocity of nanofluid, respectively.

Finally, heat exchanger effectiveness is [29]:

$$\varepsilon = \frac{\Delta T_{min}}{\Delta T_{max}} = \frac{(Tc_o - Tc_i)}{(Th_i - Tc_i)} \quad (10)$$

Where $T_C$ and $T_h$ denote the coil and shell temperatures, respectively. Inner and outer fluids are represented by the letters $i$ and $o$, respectively.

In this study, the α-$Al_2O_3$/DW nanofluid was used. The effective properties of the α-$Al_2O_3$/DW nanofluids are defined as follows [33]:

Density:

$$\rho_{nf} = (1 - \varphi)\rho_{eff,w} + \varphi \times \rho_{eff,p} \quad (11)$$

Specific heat:

$$C_{P_{nf}} = \frac{(1-\varphi)\left(\rho_{eff} c_{p_{eff}}\right)_w + \varphi\left(\rho_{eff} c_{p_{eff}}\right)_p}{(1-\varphi)\rho_{eff,w} + \varphi \times \rho_{eff,p}} \quad (12)$$

Thermal conductivity:

$$k_{nf} = \frac{k_p + 2k_w + 2(k_p - k_w)\varphi}{k_p + 2k_w - (k_p - k_w)\varphi} k_w \quad (13)$$

Dynamic viscosity:

$$\mu_{nf} = (1 + 2.5\varphi)\mu_{eff,w} \quad (14)$$

Thermo-physical parameters of water as a function of temperature are determined using the following relations [34], which are accurate between 273.15 K and 423.15 K:

$$\rho(T)=999.79684+0.068317355\,(T-273.15)-0.010740248\,(T-273.15)^2+0.00082140905\,(T-273.15)^{2.5}-2.3030988\times10^{-5}\,(T-273.15)^3 \quad (15)$$

$$\mu(T)=\frac{1}{557.82468+19.408782\,(T-273.15)+0.1360459\,(T-273.15)^2} \quad (16)$$

$$C_p(T)=\left[4.2174356-0.005618625\,(T-273.15)+0.0012992528\,(T-273.15)^{1.5}-0.00011535353\,(T-273.15)^2+4.14964\times10^{-6}\,(T-273.15)^{2.5}\right]\times10^3 \quad (17)$$

$$K(T)=0.5650285+0.0026363895\,(T-273.15)-0.00012516934\,(T-273.15)^{1.5}-1.5154918\times10^{-6}\,(T-273.15)^2-0.0009412945\,(T-273.15)^{0.5} \quad (18)$$

## 3. Numerical methodology

### *3.1 Domain geometry*

A diagram of the helical coil heat exchangers used in this research is shown in Fig. 4. Helical coil tubing with 10, 14.28, and 25 turns are all part of the geometry. To prepare the nanofluid, distilled water serves as the essential liquid, which $\alpha - Al_2O_3$ nanoparticles are added. Water circulates outside the shell while the nanofluid moves around within the coil. Table 3 lists the values for the geometric parameters considered in this analysis. Coiled tubes of varying pitches are simulated numerically.

### *3.2 Mesh generation*

A grid independence analysis is carried out to investigate the precision of the numerical simulation. ANSYS Fluent R20 is used to produce the mesh. As shown in Fig. 5, a free triangle-type mesh connects the helical coil and shell. The helical coil uses fine mesh for precision. Table 4 displays the outcomes for the five meshes used in the study (G1, G2, G3, and G4). The table shows that G4 and G5 give the same result, so G4 is chosen to reduce computational load.

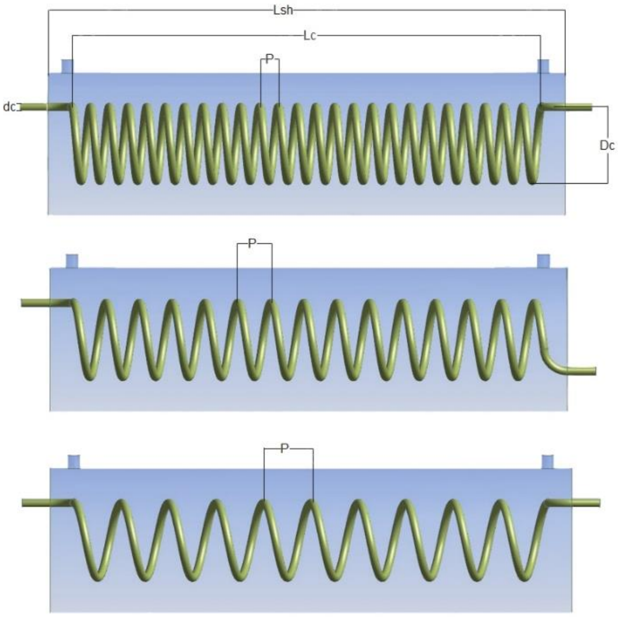


**Figure 4.** The model's helical coil heat exchangers' geometry.

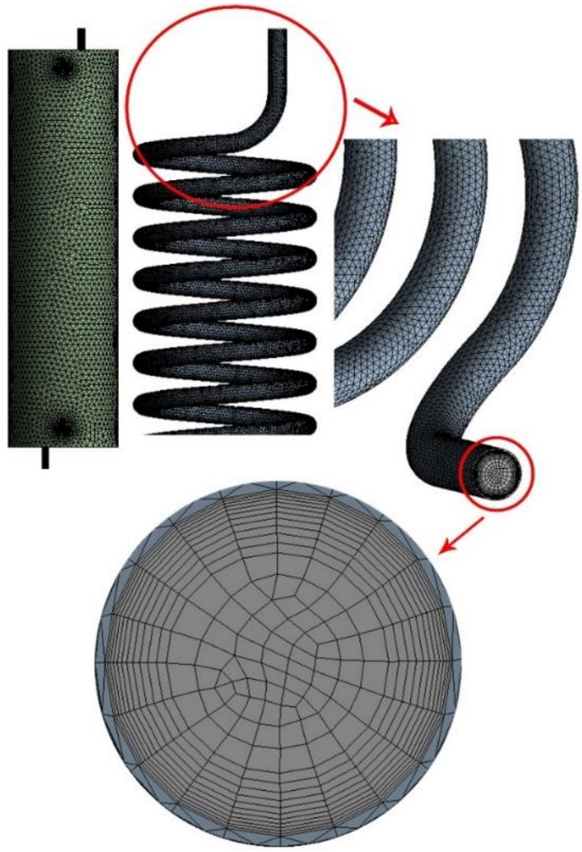

**Figure 5.** Mesh generated in the helical coil and the shell.

**Table 3:** Domain parameters.

| **Study field** | $D_c$ $(m)$ | $D_{sh}$ $(m)$ | $L_c$ $(m)$ | $L_{sh}$ $(m)$ | $d_{t,i}$ $(m)$ | $d_{t,o}$ $(m)$ | $p$ $(m)$ | $N$ |
|---|---|---|---|---|---|---|---|---|
| Experiment | 0.079 | 0.1524 | 0.5 | 0.55 | 0.0085 | 0.009 | 0.02, 0.035 and 0.05 | 10, 14.28 and 25 |
| Simulation | 0.079 | 0.1524 | 0.5 | 0.55 | 0.0085 | 0.009 | 0.020, 0.035 and 0.05 | 10, 14.28 and 25 |

**Table 4:** Grid independence result.

| **Grid** | **No. of element** | $\mathbf{T_{c,o}}$ | $\mathbf{T_{h,o}}$ | $\mathbf{Nu_c}$ |
|---|---|---|---|---|
| G1 | 2284351 | 57.8 | 63.6 | 74 |
| G2 | 3373465 | 57.9 | 63.7 | 70 |
| G3 | 4388259 | 58.8 | 63.9 | 71 |
| G4 | 5426653 | 58.2 | 64.4 | 68 |
| G5 | 6667849 | 58.12 | 64.5 | 67.9 |

### *3.3 Governing equations*

This section presents the governing equations for solving fluid flow and heat transfer within the computational domain. Flux field solutions are obtained by solving the governing equations, including continuity equations, momentum, and energy at a steady state for 3D [35]. In addition to this governing equation, the (Standard k–ε) turbulent model is used to simulate turbulent flow due to the high velocities used in this investigation; the Reynolds number is over 10000, indicating a turbulent flow, which is represented by Equation 22-24 [36]. These equations are summarized as follows:

Continuity equation:

$$\frac{\partial(\rho u_i)}{\partial x_i} = 0 \tag{19}$$

Momentum equation:

$$\frac{\partial(\rho u_i u_k)}{\partial x_i} = \frac{\partial\left(\mu \frac{\partial u_k}{\partial x_i}\right)}{\partial x_i} - \frac{\partial p}{\partial x_k} \tag{20}$$

Energy equation:

$$\frac{\partial(\rho u_i t)}{\partial x_i} = \frac{\partial\left(\frac{K}{C_p}\frac{\partial t}{\partial x_i}\right)}{\partial x_i} \tag{21}$$

Turbulent kinetic energy:

$$\frac{\partial(\rho k)}{\partial t} + \mathrm{div}(\rho k U) = \mathrm{div}\left[\frac{\mu_t}{\delta_k}\mathrm{grad}\ k\right] + 2\mu_t S_{ij} \cdot S_{ij} - \rho\varepsilon \tag{22}$$

Where

$$\mu_t = C\rho\vartheta l = \rho C_\mu \frac{k^2}{\varepsilon} \tag{23}$$

Energy dissipation rate

$$\frac{\partial(\rho\varepsilon)}{\partial t} + \mathrm{div}(\rho\varepsilon U) = \mathrm{div}\left[\frac{\mu_t}{\delta_\varepsilon}\mathrm{grad}\ \varepsilon\right] + C_{1\varepsilon}\frac{\varepsilon}{k}2\mu_t S_{ij} \cdot S_{ij} - C_{2\varepsilon}\rho\frac{\varepsilon^2}{k} \tag{24}$$

Where the empirical constants of the Standard k–ε model are given as follows:

$C_\mu=0.09$ , $\delta_k=1$ , $\delta_\varepsilon=1.3$ , $C_{1\varepsilon}=1.44$ , $C_{2\varepsilon}=1.92$

*3.4. Boundary conditions*

Mass flow rate and temperature distributions are specified as the inlet boundary conditions. The outlet's (gauge pressure = 0) value was set. In addition, a no-slip state is established on the wall. The outside walls of the shell side are regarded as adiabatic, as shown in Fig. 6, whereas the coil walls are subject to the requirement of coupling heat transfer. In addition, the disturbance intensity and hydraulic dimensions for the inlets and outlets of the two sides were determined. The hydraulic diameter of the coil side was considered equal to the coil's interior diameter, and the hydraulic diameter of the shell side was deemed equivalent to the shell diameter. The core turbulence intensity of a fully developed duct flow may be predicted using the following empirical correlation for a pipe flow-derived equation [37]:

$$I = 0.16 \times Re_{Dh}^{-1/8} \tag{25}$$

The heat exchanger's operating conditions were assumed to be as follows:

- Three-dimension model.
- The nanofluid remains a single-phase, steady-state flow and is incompressible.
- Neglecting gravity, radiation heat transfer, and viscous dissipation.
- Constant heat flux at the heat exchanger wall
- Fluid properties vary with temperature.

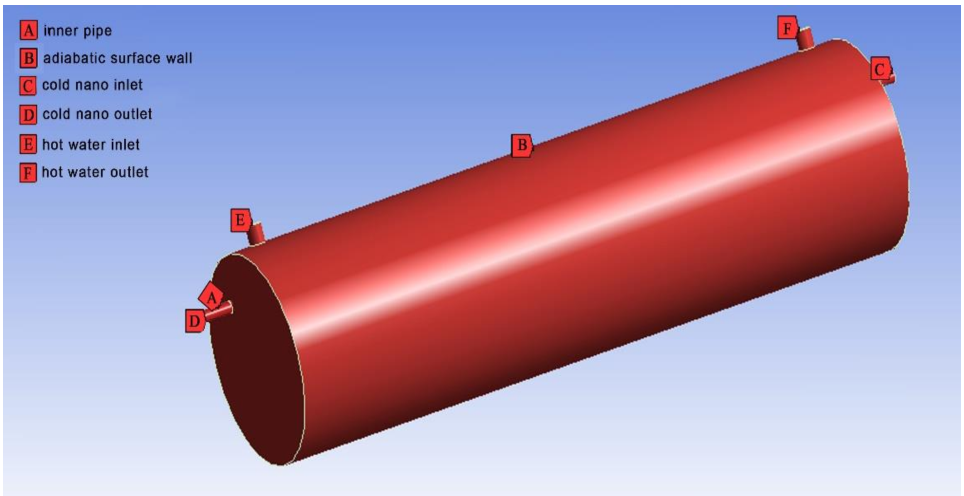


**Figure 6.** The numerical study of 3D domain's boundary conditions.

## 4. Results and discussion

### *4.1. Verification*

A discussion of the results of both numerical and experimental studies is presented in this section. The first section includes the validation of the results. Fig. 7A compares the experimental data reported by Mokhtari et al. [38], Wu et al. [39], Jayakumar et al. [40], and Fig. 7B Pawar et al. [41], Janssen & Hoogendoorn [42], and Beigzadeh & Rahimi [43] to the numerical results obtained in the present study in terms of the internal Nusselt Number. There is substantial agreement between the current research and the conclusions published in [38–43]. Here, we address the findings of both numerical and experimental investigations. The results of the current work agree well with those reported in [38-43], as shown in the Figures. A satisfactory agreement is indicated by the fact that the most significant disparity between the numerical results and the experimental findings of this work is approximately 9.94%. Regarding friction factor, Fig. 8 shows the relationships found by Beigzadeh & Rahimi [43] and Itō [44] compared to this study's numerical and theoretical results. The results of this work are consistent with [43] and [44].

Next, Fig. 9 contrasts the computational findings with the experimental results obtained for a nanoparticle size of 0.1%. The image demonstrates the high degree of consensus among the findings. Here, the highest error is just around 9.61%; therefore, the numerical modeling is accurate.

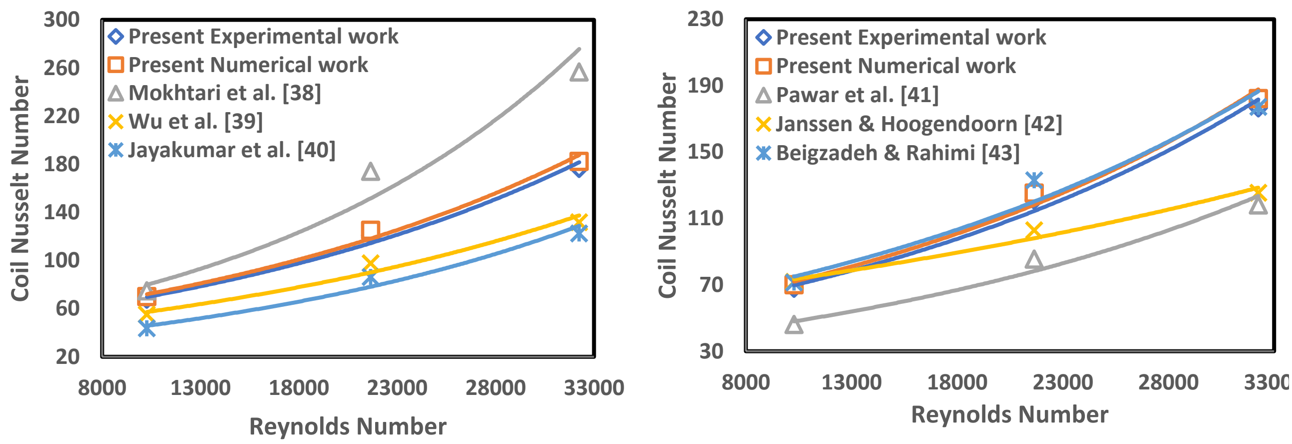


(a) (b)

**Figure 7.** Present experimental and numerical Nusselt Number results with a) [38-40] b) [41-43]

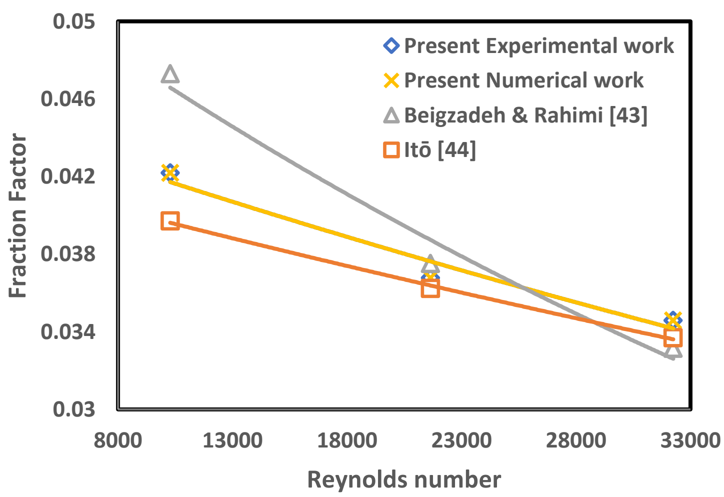


**Figure 8.** Present experimental and numerical friction factor results with [43] & [44].

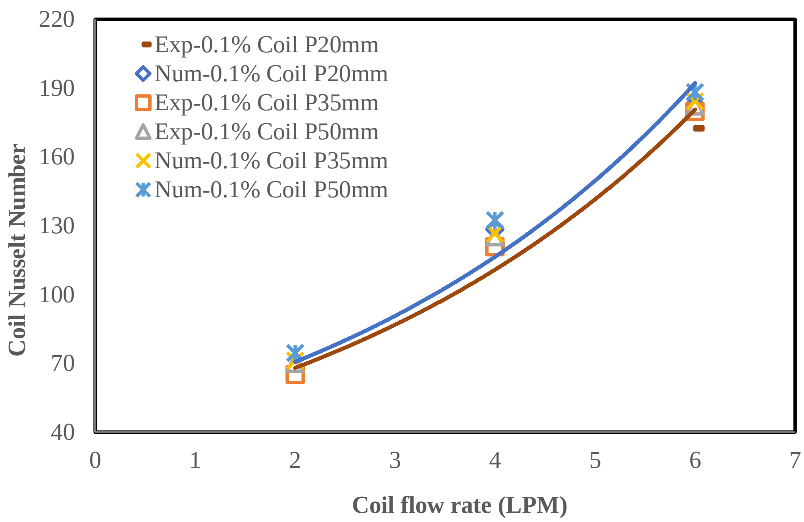


**Figure 9.** Experimental and numerical comparison of three helical pitches at 0.1% volume concentration

*4.2 The distributions of velocity and temperature*

As shown in Fig. 10, the velocity distribution in a cross-section of the three heat exchangers with varying pitch is demonstrated for a range of Reynolds numbers. As was previously mentioned, the maximum velocity in a helically coiled heat exchanger is found at the tube's outside radius rather than its center, as is the case with a straight tube. Furthermore, the secondary flow within the coil increases the heat transfer rate. Such a flow, however, increases turbulence and, by extension, friction.

The temperature profile in the cross-section of heat exchangers and helical coils of varying pitch and Reynolds number is depicted in Fig. 11. As can be seen, the hot water enters the exchanger (on the shell side), undergoes a temperature reduction as a result of heat exchange with the cold liquid on the coil side, and then exits the exchanger at a cooler temperature. In contrast, the end of the coil experiences a more significant temperature increase than the beginning due to the more substantial temperature gradient.

*4.3 The impact of volume concentration nanoparticle*

*4.3.1 Heat transfer on the inner side of the coil*

Figs. 12 and 13 depict how the nanoparticle volume percentage affects the heat transfer coefficient (h) increase and the internal Nusselt number of the coil, respectively. At a constant temperature and flow rate at the shell side, it is observed that an increase in the flow rate on the coil side considerably raises the average heat transfer coefficient (h) and, thus, the Nusselt number. This is because turbulence in the flow within the tube increases the Reynolds number and the intensity, significantly raising the (h) of the heat exchanger. Increasing the Nusselt number of nanofluids, for instance, is not very evident at a low coil flow rate (Qc = 2 LPM), yet the number improves overall by 1.99%. Adding nanoparticles to the base fluid, in this case, $\alpha - Al_2O_3$/DW is excellent for enhancing the coil flow rate. For instance, at (Qc = 6 LPM), the Nusselt number is improved by about 7.72% compared to distilled water. This is primarily due to the nanofluid's dramatically enhanced heat gain.

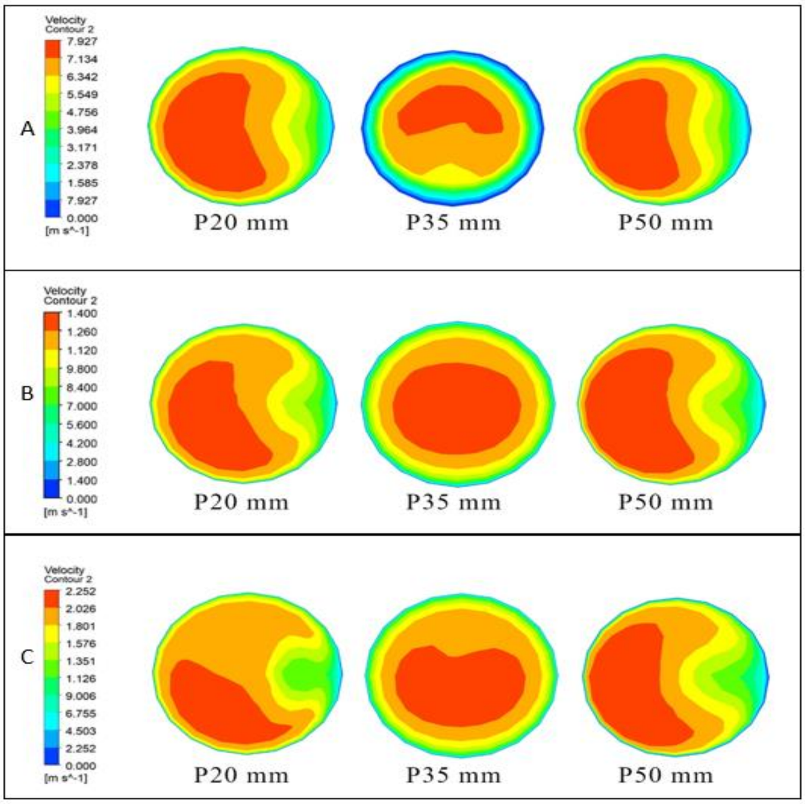


**Figure 10.** Velocity distribution in the helical coil cross-section at flow rates (A) 2 LPM (B) 4 LPM (C) 6 LPM

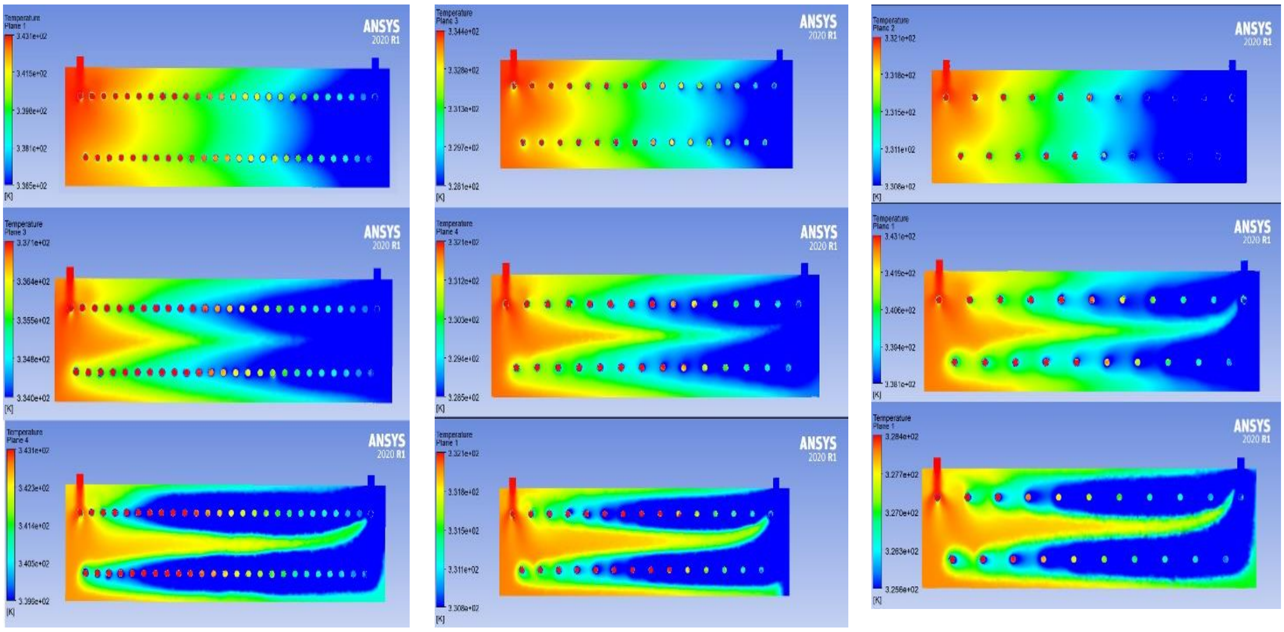


a) b) c)

**Figure 11.** Temperature distribution for (a) Coil 1, (b) Coil 2, (c) Coil 3

On the effective volume fraction of nanoparticles on the (h), as was to be predicted, the incorporation of nanoparticles would result in an increase in (h) at all Reynolds numbers. Maximum heat transfer occurs at a volume percentage of 0.1% (h = 13470.97 W/m$^2$.K)), indicating a 7.45% improvement over $\alpha - Al_2O_3$/DW in terms of heat transfer.

### *4.4 Impacts of Coil Pitch on Heat Transfer*

Fig. 14 depicts the correlation between the Reynolds number and the volume concentration of the nanofluid, together with the Nusselt number for the flow inside coils 1 (with a pitch of 25), 2 (with a pitch of 35), and 3 (with a pitch of 50). The Figure shows that the flow pattern within coil 3, characterized by the most substantial pitch gap, demonstrates a higher Nusselt number, implying a more efficient heat transfer rate. Nevertheless, this phenomenon becomes more evident when observing larger Reynolds numbers. As an example, with a constant Reynolds number of 28525, the Nusselt numbers for coils 1, 2, and 3 with a nanofluid volume concentration of 0.1% are determined to be 172.42, 179.90, and 182.22, respectively. However, when the Reynolds number reaches 10280, the Nusselt number exhibits corresponding improvements of 64.89, 65.19, and 70. The observed pattern, characterized by large centrifugal forces, can be attributed to buoyancy, which primarily influences the flow structure under high Reynolds numbers. An object's pitch also impacts the centrifugal force exerted on a fluid in motion. Consequently, secondary flows inside the pipe's cross-sectional area will be affected.

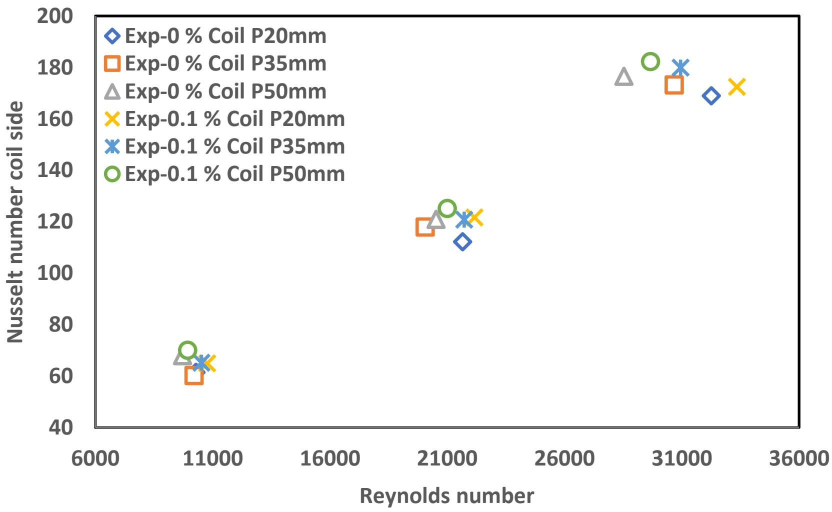


**Figure 12.** Nusselt number variations in terms of Reynolds number for various coil pitches and coil flow rates on the inner coil side.

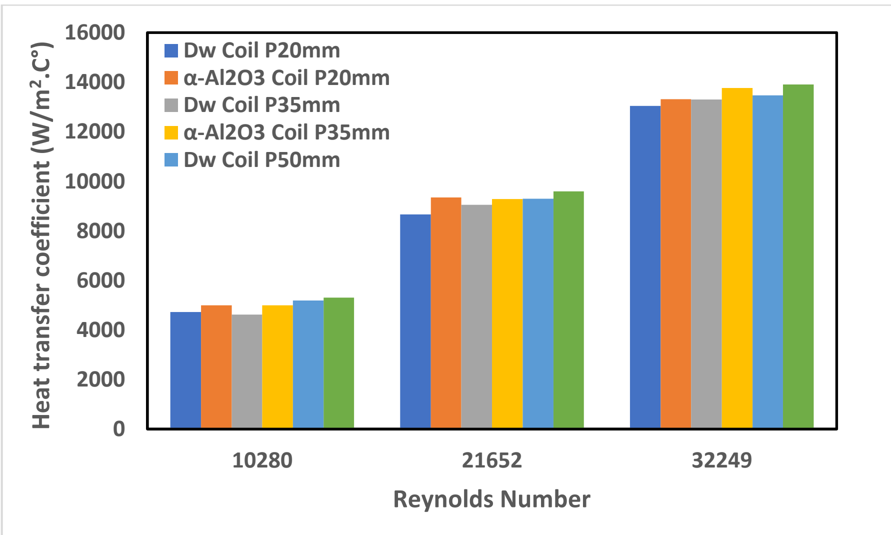


**Figure 13.** Heat transfer coefficient variations in terms of Reynolds number for various coil pitches and coil flow rates on the inner coil side.

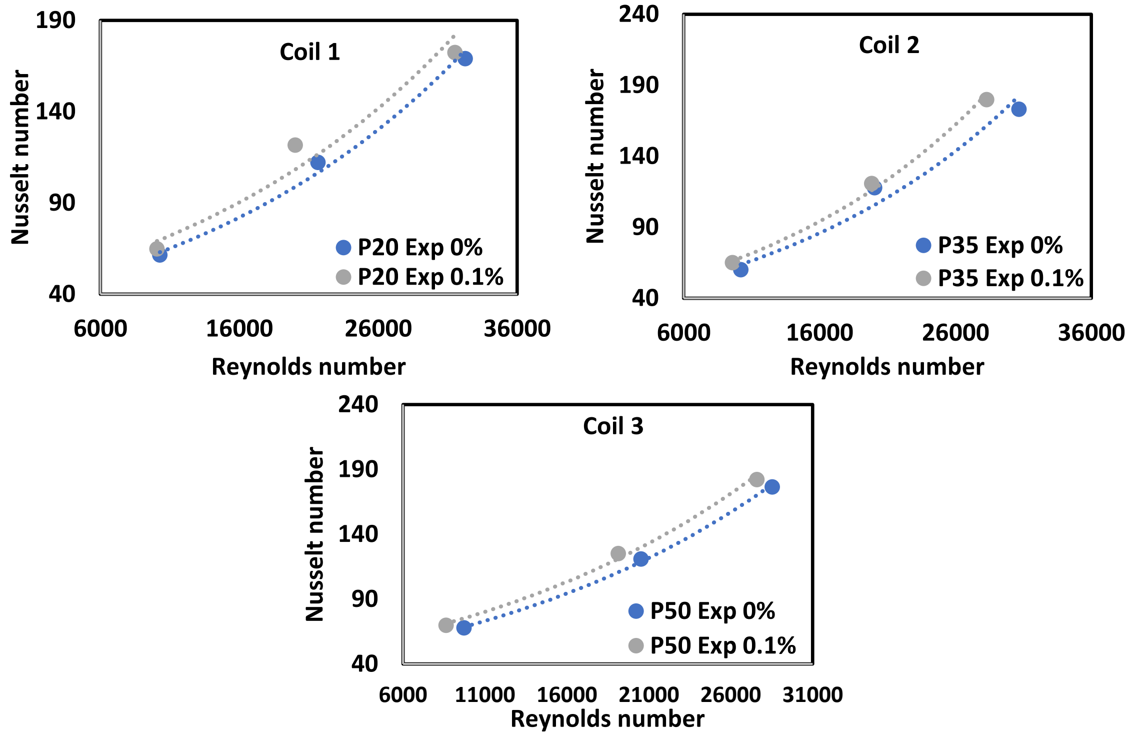


**Figure 14.** The effect of pitch spacing on heat transfer for the three coils

*4.5 Impacts of coil pitch on friction factor*

Unlike the Nusselt number, the friction factor tends to decrease as the profile side of the Reynolds number increases. Fig. 15 shows that the friction factor decreases in the helical coil at coil 3 when the coil side Reynolds number increases from 10000 to 32250. The friction factor decreases from 0.04161 to 0.033337 under the stator's coil pitch (p = 50 mm) as the Reynolds number rises. When the friction factor decreases, the Reynolds number increases from 10,000 to 32,250. The reason is that an increase in the Reynolds number will increase the flow rate, which leads to an increase in the velocity. Moreover, the friction factor exhibits an inverse relationship with the flow rate, reducing the friction factor as the flow rate increases.

*4.6 Impacts of coil pitch on pressure drop*

Fig. 16 illustrates the impact of nanofluid (α- $Al_2O_3$) and the pitch ratio of the helical tube on pressure drop. A concentration of just 0.1% of (α- $Al_2O_3$) nanoparticles leads to notable pressure differences. At Reynolds number 10280, pressure reductions of 1.31%, 4.76%, and 6.45% were observed compared to distilled water. The maximum pressure drop measured was 37231.65 Pa for distilled water and 38610.6 Pa for α-$Al_2O_3$ at a 0.1% volumetric concentration and Reynolds number 32250. The Figure shows that as the Reynolds number rises, the flow becomes more turbulent, resulting in increased momentum transfer and a greater pressure drop. The presence of nanoparticles (α- $Al_2O_3$) in the nanofluid elevates its viscosity, introducing additional resistance to flow. Consequently, the pressure drop when using nanofluid (α- $Al_2O_3$) rises more rapidly with increasing Reynolds number compared to distilled water.

## 5. Nusselt number estimate correlation

Using a least-squares power-law fit experimental data, we find the following correlation, with a corrected correlation coefficient $R^2$ = 99.46%, that may be used to determine the Nusselt number of nanofluid flow within the helical coils.

$$Nu_c = 0.023Re^{0.8}Pr^{0.4}\gamma^{-0.08} \qquad (26)$$

The parameters' ranges are as follows: $10000 \leq Re \leq 32250$, $2.88 \leq Pr \leq 3.33$, and $0.080625655 \leq \gamma \leq 0.201564138$. The Nusselt numbers, as depicted in Fig. 17, exhibit a deviation of -4.87% to +4.30% from the corresponding experimental values.

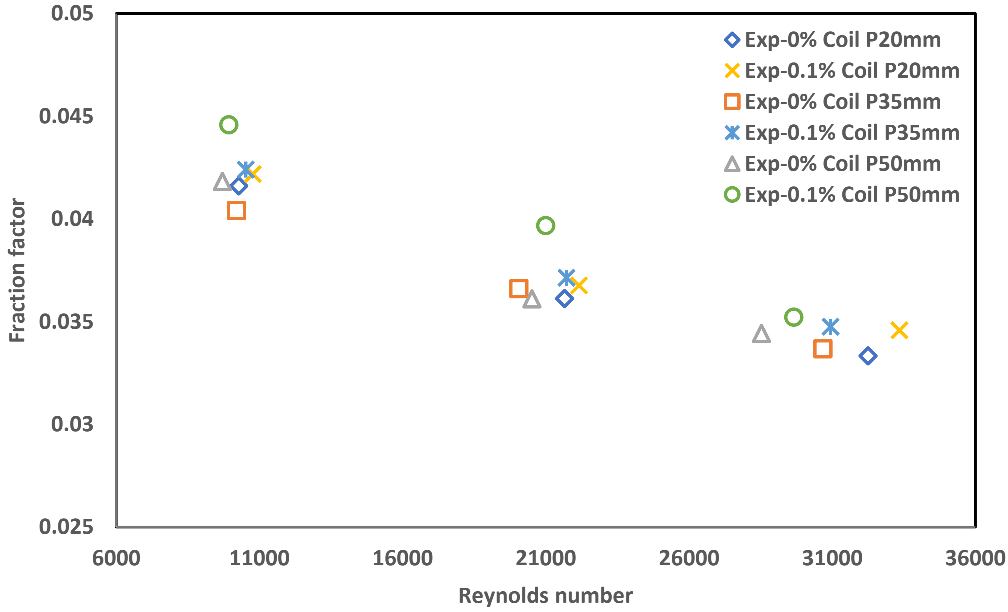


**Figure 15.** Coil Pitch effect on friction factor for the three coils.

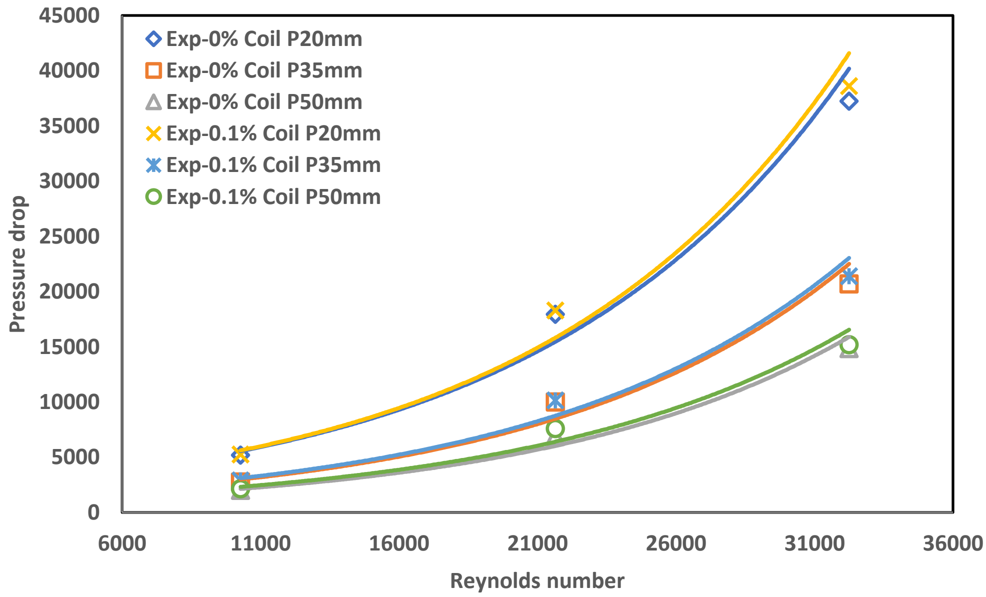


**Figure 16.** Pressure drop variations in terms of Reynolds number for various coil pitches and coil flow rates on the inner coil side.

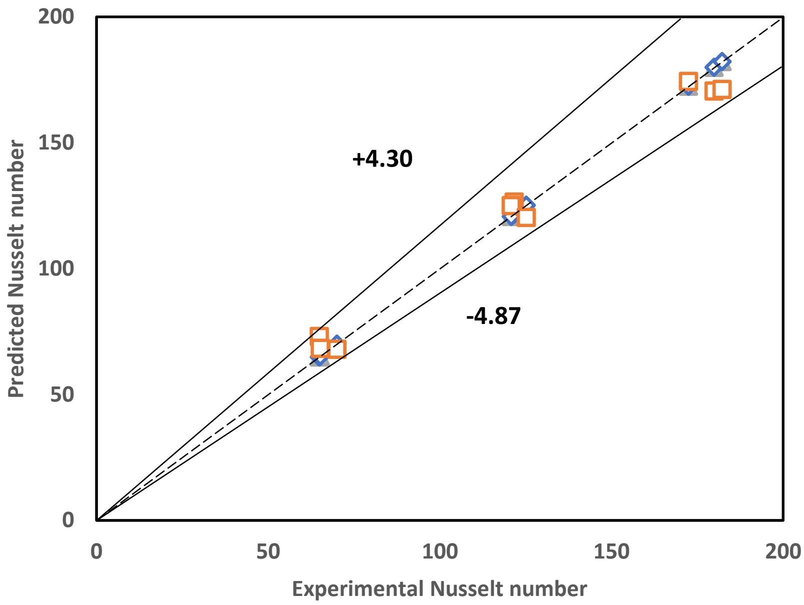


**Figure 17.** Coil-side Nusselt number comparison between experiment and predicted.

## 4. Conclusions

In the current study, experiments and computer simulations were used to study the heat transfer coefficients of shell and helical coil tube heat exchangers using a small volume concentration of nanofluid $\alpha - Al_2O_3$, which is 0.1%. Three heat exchangers with different coil pitches were tested in parallel and counter-flow configurations. Experimental and numerical settings are explained, and results from a range of flow rates on the coil side of the system (i.e., Nusselt number and heat transfer coefficient) were compiled. Moreover, a comprehensive investigation has been undertaken to examine several facets, such as the influence of coil pitches on heat transfer and the friction factor on the coil side. The following results provide many conclusions:

- In counter-flow setups, the Nusselt numbers on the coil side exceeded those observed in parallel-flow arrangements.
- The heat transfer coefficients for larger pitch coils were notably higher than those for smaller ones on the coil side.
- The heat transfer coefficient and the heat transfer rate of a heat exchanger are enhanced when a nanofluid is used instead of water. These coefficients grow as the nanofluid's velocity increases.
- The third coil, featuring a 50mm pitch and a flow rate of 6 LPM, achieved the highest heat transfer coefficient, measuring 13,471 W/m$^2$.C°. This result indicated a 7.45% enhancement over the base fluid's performance.
- The highest Nusselt number was observed when a nanofluid with a 0.1% volume concentration flowed at a rate of 6 LPM through coil 3, spaced 50mm apart, resulting in a value of 182.22. This represented a 7.72% enhancement compared to a liquid based on water.
- Maximum friction occurred at 2 LPM of fluid flow within coil 3 with a 50mm pitch and a friction factor of 0.044587. On the other hand, under the identical flow rate settings, the coil with a pitch of 20mm, denoted as coil 1, exhibited the minimum value of 0.03333.

## References

[1] P.K. Sahoo, M.I.A. Ansari, A.K. Datta, A computer based iterative solution for accurate estimation of heat transfer coefficients in a helical tube heat exchanger, J. Food Eng. 58 (2003) 211–214. https://doi.org/10.1016/S0260-8774(02)00370-9.

[2] S. Chingulpitak, S. Wongwises, A comparison of flow characteristics of refrigerants flowing through adiabatic straight and helical capillary tubes, Int. Commun. Heat Mass Transf. 38 (2011) 398–404. https://doi.org/10.1016/j.icheatmasstransfer.2010.12.014.

[3] W.H. Park, C.K.K. Yang, Effects of using advanced cooling systems on the overall power consumption of processors, IEEE Trans. Very Large Scale Integr. Syst. 21 (2013) 1644–1654. https://doi.org/10.1109/TVLSI.2012.2217386.

[4] H. Ma, N. Du, Z. Zhang, F. Lyu, N. Deng, C. Li, S. Yu, Assessment of the optimum operation conditions on a heat pipe heat exchanger for waste heat recovery in steel industry, 79 (2017) 50–60. https://doi.org/10.1016/j.rser.2017.04.122.

[5] B.A. Bhanvase, S.D. Sayankar, A. Kapre, P.J. Fule, S.H. Sonawane, Experimental investigation on intensified convective heat transfer coefficient of water based PANI nanofluid in vertical helical coiled heat exchanger, Appl. Therm. Eng. 128 (2018) 134–140. https://doi.org/10.1016/j.applthermaleng.2017.09.009.

[6] F. Ahmed, Experimental investigation of Al2O3-water nanofluid as a secondary fluid in a refrigeration system, Case Stud. Therm. Eng. 26 (2021) 101024. https://doi.org/10.1016/j.csite.2021.101024.

[7] S.M. Elshamy, M.T. Abdelghany, M.R. Salem, O.E. Abdellatif, Energy and exergy analysis of shell and coil heat exchanger using water based Al2O3 nanofluid including diverse coil geometries: An experimental study, J. Nanofluids. 9 (2020) 13–23. https://doi.org/10.1166/JON.2020.1727.

[8] A. Al-damook, Multi-objective numerical optimum design of natural convection in different configurations of concentric horizontal annular pipes using different nanofluids, (n.d.).

[9] P.W. Sunu, D.S. Anakottapary, I.D.M. Susila, I.D.M.C. Santosa, I.N.E. Indrayana, Study of thermal effectiveness in shell and helically coiled tube heat exchanger with addition nanoparticles, J. Phys. Conf. Ser. 1569 (2020) 1–5. https://doi.org/10.1088/1742-6596/1569/3/032038.

[10] B.A.K. Naik, A.V. Vinod, Heat transfer enhancement using non-Newtonian nanofluids in a shell and helical coil heat exchanger, Exp. Therm. Fluid Sci. 90 (2018) 132–142. https://doi.org/10.1016/j.expthermflusci.2017.09.013.

[11] F. Hormozi, B. ZareNezhad, H.R. Allahyar, An experimental investigation on the effects of surfactants on the thermal performance of hybrid nanofluids in helical coil heat exchangers, Int. Commun. Heat Mass Transf. 78 (2016) 271–276. https://doi.org/10.1016/j.icheatmasstransfer.2016.09.022.

[12] M. Kahani, S. Zeinali Heris, S.M. Mousavi, Comparative study between metal oxide nanopowders on thermal characteristics of nanofluid flow through helical coils, Powder Technol. 246 (2013) 82–92. https://doi.org/10.1016/j.powtec.2013.05.010.

[13] F. Ahmed, T. Syed, Numerical Investigation of Heat Transfer Rate in Helically Coiled Pipe Using Al2O3/Water Nanofluid, Diyala J. Eng. Sci. 13 (2020) 27–36. https://doi.org/10.24237/djes.2020.13404.

[14] M.J. Hasan, S.F. Ahmed, A.A. Bhuiyan, Geometrical and coil revolution effects on the performance enhancement of a helical heat exchanger using nanofluids, Case Stud. Therm. Eng. 35 (2022) 102106. https://doi.org/10.1016/j.csite.2022.102106.

[15] M. Zaboli, S. Saedodin, S.S. Mousavi Ajarostaghi, M. Nourbakhsh, Numerical evaluation of the heat transfer in a shell and corrugated coil tube heat exchanger with three various water-based nanofluids, Heat Transf. 50 (2021) 6043–6067. https://doi.org/10.1002/htj.22161.

[16] M. Zaboli, S.S.M. Ajarostaghi, M. Noorbakhsh, M.A. Delavar, Effects of geometrical and operational parameters on heat transfer and fluid flow of three various water based nanofluids in a shell and coil tube heat exchanger, SN Appl. Sci. 1 (2019). https://doi.org/10.1007/s42452-019-1431-2.

[17] I.D.J. Azzawi, S.G. Yahya, L.A.H. Al-rubaye, S.K. Ali, Heat Transfer Enhancement of Different Channel Geometries Using Nanofluids and Porous Media, 39 (n.d.) 1197–1206.

[18] S.K. Ali, I.D.J. Azzawi, A.A. Khadom, Evaluation Analysis of Double Coil Heat Exchanger for Heat Transfer Enhancement, 8716 (1999) 96–107. https://doi.org/10.24237/djes.2021.14109.

[19] S. Kh, I.D.J. Azzawi, A.A. Khadom, Experimental validation and numerical investigation for optimization and evaluation of heat transfer enhancement in double coil heat exchanger, Therm. Sci. Eng. Prog. 22 (n.d.) 100862. https://doi.org/10.1016/j.tsep.2021.100862.

[20] M. Omidi, M. Farhadi, A. Ali Rabienataj Darzi, Numerical study of heat transfer on using lobed

cross sections in helical coil heat exchangers: Effect of physical and geometrical parameters, Energy Convers. Manag. 176 (2018) 236–245. https://doi.org/10.1016/j.enconman.2018.09.034.

[21] A.M. Fsadni, J.P.M. Whitty, M.A. Stables, A.A. Adeniyi, Numerical study on turbulent heat transfer and pressure drop characteristics of a helically coiled hybrid rectangular-circular tube heat exchanger with Al2O3-water nanofluids, Appl. Therm. Eng. 114 (2017) 466–483. https://doi.org/10.1016/j.applthermaleng.2016.11.181.

[22] S. Bahrehmand, A. Abbassi, Heat transfer and performance analysis of nanofluid flow in helically coiled tube heat exchangers, Chem. Eng. Res. Des. 109 (2016) 628–637. https://doi.org/10.1016/j.cherd.2016.03.022.

[23] V. Sisodiya, D.A. Geete, Heat Transfer Analysis of Helical Coil Heat Exchanger With Al2O3 Nano Fluid, Int. Res. J. Eng. Technol. 3 (2016) 366–370. www.irjet.net.

[24] W.I.A. Aly, Numerical study on turbulent heat transfer and pressure drop of nanofluid in coiled tube-in-tube heat exchangers, Energy Convers. Manag. 79 (2014) 304–316. https://doi.org/10.1016/j.enconman.2013.12.031.

[25] A.A.R. Darzi, M. Farhadi, K. Sedighi, S. Aallahyari, M.A. Delavar, Turbulent heat transfer of Al2O3-water nanofluid inside helically corrugated tubes: Numerical study, Int. Commun. Heat Mass Transf. 41 (2013) 68–75. https://doi.org/10.1016/j.icheatmasstransfer.2012.11.006.

[26] A.F. Faraj, I.D.J. Azzawi, S.G. Yahya, Pitch Variations Study on Helically Coiled Pipe in Turbulent Flow Region Using CFD, 38 (n.d.) 775–784.

[27] K.M. Elshazly, R.Y. Sakr, R.K. Ali, M.R. Salem, Effect of γ-Al2O3/water nanofluid on the thermal performance of shell and coil heat exchanger with different coil torsions, Heat Mass Transf. Und Stoffuebertragung. 53 (2017) 1893–1903. https://doi.org/10.1007/s00231-016-1949-4.

[28] J.P. Holman, Experimental Methods for Engineers, McGraw-Hill, 2001.

[29] R.K. Shah, D.P. Sekulic, FUNDAMENTALS OF HEAT EXCHANGER DESIGN, John Wiley & Sons, 2003.

[30] H.M. Maghrabie, M. Attalla, A. A. A. Mohsen, Performance assessment of a shell and helically coiled tube heat exchanger with variable orientations utilizing different nanofluids, Appl. Therm. Eng. 182 (2021) 116013. https://doi.org/10.1016/j.applthermaleng.2020.116013.

[31] A. Sheeba, C.M. Abhijith, M. Jose Prakash, Experimental and numerical investigations on the heat transfer and flow characteristics of a helical coil heat exchanger, Int. J. Refrig. 99 (2019) 490–497. https://doi.org/10.1016/j.ijrefrig.2018.12.002.

[32] A.H. Shiravi, M. Shafiee, M. Firoozzadeh, H. Bostani, M. Bozorgmehrian, Experimental study on convective heat transfer and entropy generation of carbon black nanofluid turbulent flow in a helical coiled heat exchanger, J. Therm. Anal. Calorim. 145 (2021) 597–607. https://doi.org/10.1007/s10973-020-09729-1.

[33] M. Kahani, S.Z. Heris, S.M. Mousavi, Effects of Curvature Ratio and Coil Pitch Spacing on Heat Transfer Performance of Al2O3/Water Nanofluid Laminar Flow through Helical Coils, J. Dispers. Sci. Technol. 34 (2013) 1704–1712. https://doi.org/10.1080/01932691.2013.764485.

[34] C.O. Popiel, J. Wojtkowiak, Simple formulas for thermophysical properties of liquid water for heat transfer calculations (from 0°c to 150°c), Heat Transf. Eng. 19 (1998) 87–101. https://doi.org/10.1080/01457639808939929.

[35] O. Prakash, K. Jha, Effect of MWCNT Water Nanofluid on Heat Transfer Enhancement in a Shell and coiled Tube Exchanger using CFD, Int. J. Trend Sci. Res. Dev. 4 (2020) 1004–1014.

[36] H.K. Versteeg, W. Malalasekera, An Introduction to Parallel Computational Fluid Dynamics, Second Edi, Pearson Education Limited, London, 2007.

[37] A. Alimoradi, F. Veysi, Prediction of heat transfer coefficients of shell and coiled tube heat exchangers using numerical method and experimental validation, Int. J. Therm. Sci. 107 (2016) 196–208. https://doi.org/10.1016/j.ijthermalsci.2016.04.010.

[38] A. Mokhtari Ardekani, V. Kalantar, M.M. Heyhat, Experimental study on heat transfer enhancement of nanofluid flow through helical tubes, Adv. Powder Technol. 30 (2019) 1815–1822. https://doi.org/10.1016/j.apt.2019.05.026.

[39] Z. Wu, L. Wang, B. Sundén, Pressure drop and convective heat transfer of water and nanofluids in a double-pipe helical heat exchanger, Appl. Therm. Eng. 60 (2013) 266–274. https://doi.org/10.1016/j.applthermaleng.2013.06.051.

[40] J.S. Jayakumar, S.M. Mahajani, J.C. Mandal, P.K. Vijayan, R. Bhoi, Experimental and CFD estimation of heat transfer in helically coiled heat exchangers, Chem. Eng. Res. Des. 86 (2008) 221–232.

https://doi.org/10.1016/j.cherd.2007.10.021.

[41] S.S. Pawar, V.K. Sunnapwar, Experimental studies on heat transfer to Newtonian and non-Newtonian fluids in helical coils with laminar and turbulent flow, Exp. Therm. Fluid Sci. 44 (2013) 792–804. https://doi.org/10.1016/j.expthermflusci.2012.09.024.

[42] L.A.M. Janssen, C.J. Hoogendoorn, Laminar convective heat transfer in helical coiled tubes, Int. J. Heat Mass Transf. 21 (1978) 1197–1206. https://doi.org/10.1016/0017-9310(78)90138-2.

[43] R. Beigzadeh, M. Rahimi, Prediction of thermal and fluid flow characteristics in helically coiled tubes using ANFIS and GA based correlations, Int. Commun. Heat Mass Transf. 39 (2012) 1647–1653. https://doi.org/10.1016/j.icheatmasstransfer.2012.10.011.

[44] H. Itō, Friction Factors for Turbulent Flow in Curved Pipes, J. Basic Eng. 81 (1959) 123–132. https://doi.org/10.1115/1.4008390.

## Nomenclature

| Symbol | Description | Symbol | Description |
|---|---|---|---|
| $Al_2O_3$ | Aluminum oxide | P | Pitch (m) |
| $SiO_2$ | Silicon dioxide | d $(m)$ | Tube diameter, $m$ |
| Ag | Silver | $D_c(m)$ | Diameter of coil, $m$ |
| ZnO | Zinc oxide | $\dot{m}$ | Flow rate, $kg/s$ |
| CuO | Cupric Oxide | $h$ | Heat transfer coefficient, $W/m^2.K$ |
| $TiO_2$ | Titanium dioxide | LPM | Litre per minutes |
| MWCNT | Multi-walled carbon nanotubes | $Nu$ | Nusselt number |
| A | Area, $mm^2$ | $Pr$ | Prandtl number |
| $C_p$ | Specific heat, $J/kg.K$ | $Re$ | Reynolds number |
| k | Thermal conductivity, $W/m.K$ | LMTD | Logarithmic mean temperature difference |
| µ | Dynamic viscosity | $L$ | Shell and coil length, $m$ |
| COP | Coefficient of performance | $U$ | Overall heat transfer coefficient, $W/m^2.$℃ |
| Dw | Distilled water | vol% | volume percent |
| N | Number of turns | wt% | Weight percent |
| | ***Greek Letters*** | | |
| $\rho$ | Density, $kg/m^3$ | $\lambda$ | Coil torsion, Pc/ π Dc |
| $\varphi$ | Volume fraction of nanoparticles | α | Alpha |
| $\mu$ | Dynamic viscosity, $Pa.s$ | η | efficiency |
| $\varepsilon$ | Effectiveness | | |
| | ***Subscripts*** | | |
| $c$ | Coil or cold fluid | $o$ | Outlet |
| $h$ | Hot fluid | t | Tube |
| $i$ | Inner or internal | ex | exergy |